Journal of the Physical Society of Japan
Vol. 70, No. 3, March, 2001, pp. 617–620

Power Absorption Calculation for Electron Cyclotron Resonance Heating in H-1 Heliac

Kazunobu NAGASAKI*, Michael G. SHATS, Helen SMITH and Horst PUNZMANN

Plasma Research Laboratory, Research School of Physical Sciences and Engineering, The Australian National University, Canberra, ACT 0200, Australia

(Received July 5, 2000)

Power absorption is calculated for electron cyclotron resonance heating (ECRH) in the H-1 heliac device by using a ray tracing numerical code. The three-dimensional magnetic field structure and the bean shape of flux surfaces are considered. The calculation results show that the second harmonic extraordinary mode heating is effective even at low density if the launching direction is properly adjusted. The localized power absorption profile can be shifted from on-axis to off-axis by controlling the magnetic field strength or the launching angle, making the heat transport experiment possible.

KEYWORDS: electron cyclotron resonance heating, ray tracing calculation, heliac

Electron cyclotron resonance heating (ECRH) has been recognized as an effective scheme for plasma production and heating in magnetically confined plasmas. In helical systems, in particular, ECRH has been utilized for the production of current-free plasmas. The advantage of ECRH is that it allows the launching of a well-collimated millimeter wave beam with a controlled direction and polarization, which makes it possible to localize the power deposition and control its radial position.

Ray tracing calculation is an efficient method of determining the propagation and absorption of electron cyclotron waves in realistic field geometries and plasma inhomogeneities. Several numerical codes have been developed for toroidal devices such as TORAY,[1] RAYS[2] and TRECE.[3] Since the calculation results are usually found to be in good agreement with experiments, the ray tracing technique is recognized as a powerful tool for power absorption profile computations. Recently, a 28 GHz ECRH system has been installed for the H-1 heliac at the Australian National University for producing high electron temperature plasma. Due to the complex three-dimensional (3D) geometry of the confining magnetic field in H-1, the power absorption profile should be computed using the realistic magnetic configuration to characterize the propagation and absorption of the injected millimeter wave beam in the plasma.

In this Letter, we present the modeling results of the ECRH power absorption in the H-1 heliac by using a geometrical optics approximation. Dependencies on electron density, launching conditions and the magnetic field strength are shown mainly for the second harmonic extraordinary (X-) mode ECRH. Expected plasma parameters are also presented which are obtained by combining the total absorbed power with the International Stellarator Scaling 95 (ISS95) energy confinement scaling law.[4]

H-1 is a three-field period toroidal heliac (helical axis stellarator) with major radius $R_0 = 1.0\,\mathrm{m}$, averaged minor radius $a = 0.2\,\mathrm{m}$, rotational transform $\iota/2\pi = 0.6$–2.0 and low magnetic shear $\Delta\iota/\iota = 0.03$–0.06.[5,6] Flux surfaces are formed by a set of coils comprising 36 toroidal field coils, four vertical field coils, one poloidal field coil (central ring conductor) and one helical coil. In this paper, we consider one configuration characterized by $\iota/2\pi \sim 1.15$ and $R_{\mathrm{axis}} = 1.2\,\mathrm{m}$. Here R_{axis} is defined as the magnetic axis position at the toroidal angle where the flux surfaces are located outside the poloidal field coil.

A 28 GHz ECRH system has been designed and installed on the H-1 heliac. The gyrotron is a high-power millimeter wave source producing a power of 200 kW at 28 GHz, in a pulse of up to 40 msec long. It outputs the radiation as a TE_{02} mode. The TE_{02} mode is converted into the HE_{11} waveguide mode through an in-waveguide converter, the HE_{11} mode is transmitted through corrugated waveguides, and then the Gaussian beam is launched from the outside of the torus into the plasma.

A ray tracing code, 'H-RAY', has been developed to calculate the ECRH power absorption for the H-1 configuration. The H-RAY code solves the radiative transfer equations under the geometrical optics approximation. Assuming that the nonuniformity of the plasma parameters is weak and the geometrical optics approximation is valid, the wave trajectory is numerically calculated from the following set of differential equations,

$$\frac{\mathrm{d}\boldsymbol{r}}{\mathrm{d}\tau} = \frac{\partial D}{\partial \boldsymbol{k}}, \quad \frac{\mathrm{d}\boldsymbol{k}}{\mathrm{d}\tau} = -\frac{\partial D}{\partial \boldsymbol{r}}, \quad \frac{\mathrm{d}t}{\mathrm{d}\tau} = -\frac{\partial D}{\partial \omega}, \qquad (1)$$

where $D(\omega, \boldsymbol{k}, \boldsymbol{r}) = 0$ is the local dispersion relation of the wave, and $\boldsymbol{r}(\tau)$, $\boldsymbol{k}(\tau)$ and $t(\tau)$ denote the position, wave vector and time along the wave trajectory, respectively, which are related to each other through the pa-

*Permanent address: Institute of Advanced Energy, Kyoto University, Uji, Kyoto 611-0011. E-mail: nagasaki@iae.kyoto-u.ac.jp

rameter τ. In this Letter, we use the dispersion relation obtained using a cold plasma approximation.[7] The dispersion relation D is given by

$$\begin{aligned} D &= AN^4 - BN^2 + C, \\ A &= S\sin^2\theta + P\cos^2\theta, \\ B &= RL\sin^2\theta + PS(1+\cos^2\theta), \\ C &= PRL, \end{aligned} \tag{2}$$

where S, P, R and L are the Stix's notations, and θ is the angle that the magnetic field makes with the wave vector. The absorption coefficients are calculated by using a weakly relativistic approximation for the dielectric tensor (see ref. 8 for explicit expressions). The 3D magnetic field structure is taken into account in the calculation. The shape of the flux surfaces is assumed to be helically symmetric, that is, to be the same at any poloidal cross-section. This is a reasonable assumption because the shape of the flux surface is weakly dependent on the toroidal angle.

We consider two different launching geometries of the millimeter wave beam corresponding to two experimental setups: (a) horizontal launch directly from the corrugated waveguide and (b) bottom launch from the focusing mirror. In the horizontal launch case, the beam is injected from the outside of the torus in the equatorial plane. In the bottom launching case, the beam is injected from the mirror placed inside the vacuum tank at the bottom of the plasma. In both cases, we assume that the rays are divergent from the waveguide or the mirror. The $1/e^2$ power radius at the magnetic axis in the vacuum state is determined from the experimental results obtained in the low-power measurement. To model the Gaussian beam, a bunch of rays is launched with a power distribution of $P(\rho) = P(0)\exp\{-(\rho/\rho_b)^2\}$, where ρ is the beam radius on the plane perpendicular to the initial wave vector. The H-RAY code does not treat focused Gaussian beams. The geometric optics approximation breaks down at the focal point (at the waist of the millimeter wave beam), where the electric field has infinite amplitude. A rigorous description would be required for the accurate power absorption profile computation in this case. Such a mode should include diffraction effects.[9,10] Nevertheless, the conventional ray tracing code is a useful tool for calculating the power absorption profile and to optimize the launching conditions and the plasma parameters.

The electron density and temperature profiles are given by $n_e = n_e(0)\{1-(r/a)^4\}$ and $T_e(r) = T_e(0)\{1-(r/a)^2\}$, which are usually observed in the ECH plasmas on helical devices.[11] Here r is the averaged minor radius of the flux surface. It is assumed that the electron density and temperature are a function of the averaged minor radius, that is, these profiles are consistent with the flux surface shape. It should be noted that the T_e profile changes with the change in the power absorption profile. The T_e profile is usually broader when the resonance position is shifted from the axis. However, this fixed temperature profile gives us reasonable results, since the electron temperature at the resonant position, which is most important for the absorption, is not significantly affected even when moving the resonant position. Multireflection of the unabsorbed radiation from the vacuum chamber wall is not considered in the calculation. Since the walls of the vacuum chamber of H-1 are located far away from the plasma (unlikely in other toroidal plasma devices), the multireflections are less important. The number of rays used in the model is determined by evaluating the numerical error in the absorbed power deposited in a radial mesh. The grid size of 16×16 guarantees that the relative error is less than 1%.

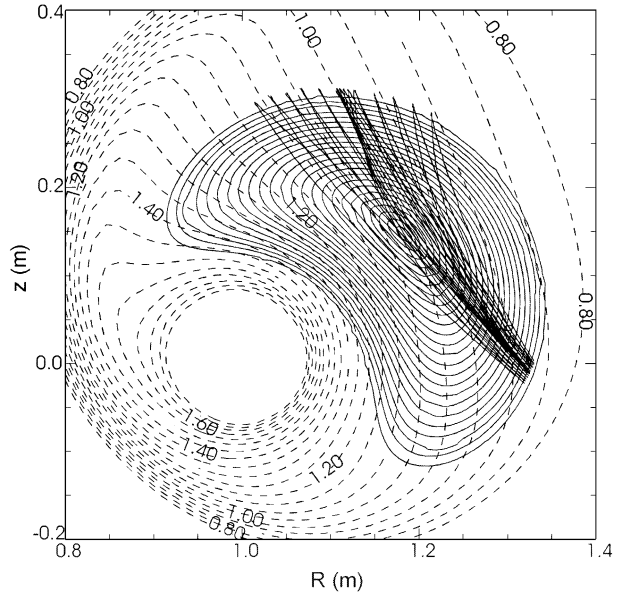

Fig. 1. Example of ray trajectories of the 28 GHz second harmonic X-mode waves. The code input parameters are $n_e(0) = 0.2 \times 10^{19}\,\mathrm{m}^{-3}$ and $B(0) = 0.5\,\mathrm{T}$. Solid and dashed contours denote the flux surfaces and the B contours, respectively.

An example of the ray trajectories in an H-1 plasma is shown in Fig. 1 for the bottom launching case in the second harmonic X-mode. The flux surfaces and B contour of the poloidal cross section of the launching port are plotted. The ray trajectories are projected onto this poloidal cross-section. As the electron density increases, the refraction effect becomes stronger, and finally the ray cannot access the resonance layer when the electron density reaches the right hand cut-off, $n_e = 0.5 \times 10^{19}\,\mathrm{m}^{-3}$, as expected.

Although the refraction is stronger for the bottom launching case (because of the longer optical path than for the horizontal launching), the higher single pass absorption is obtained. Figure 2 shows the dependence of the single pass absorption rate on the magnetic field strength. The toroidal launching angle is the same for both horizontal and bottom launching cases. While the effective magnetic field range is narrower for the bottom launching case, the absorption rate is found to be up to 82% even at low density. This is because the optical thickness is higher due to the longer optical path. Thus the bottom launching is preferable from the single pass absorption point of view.

The power absorption radial position can be controlled

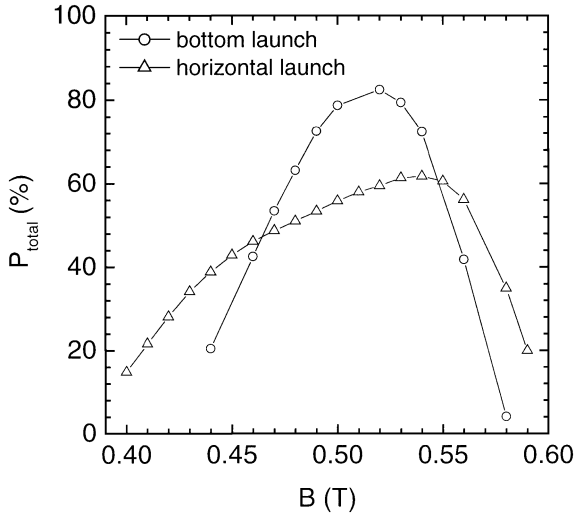

Fig. 2. B dependence of the total single-pass absorption rate. The total absorption in the horizontal launching case is plotted. The electron density and temperature are assumed to be $n_e(0) = 0.2 \times 10^{19}\,\mathrm{m}^{-3}$ and $T_e(0) = 500\,\mathrm{eV}$.

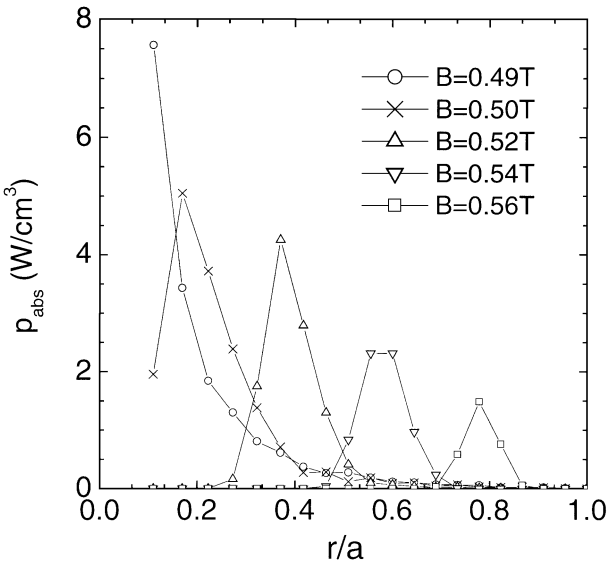

Fig. 3. Power absorption profile during the magnetic field strength scan. The electron density and temperature are the same as in Fig. 2.

by changing the magnetic field strength. Figure 3 shows the dependence of the power absorption profiles on the magnetic field strength for the bottom launching case. The poloidal and toroidal launching angles are adjusted so that the central ray crosses the magnetic axis perpendicularly to the magnetic field in vacuum. The localized power absorption can be shifted from on-axis to off-axis ($r/a = 0.6$) while keeping the total absorption rate above 70%. This suggests that the profile control and heat transport experiments would be made possible in H-1 by changing the absorption position at the second harmonic X-mode ECRH.

The poloidal launching angles have also been scanned to determine the highest single pass absorption. Figure 4 shows the contours of the single pass absorption rate

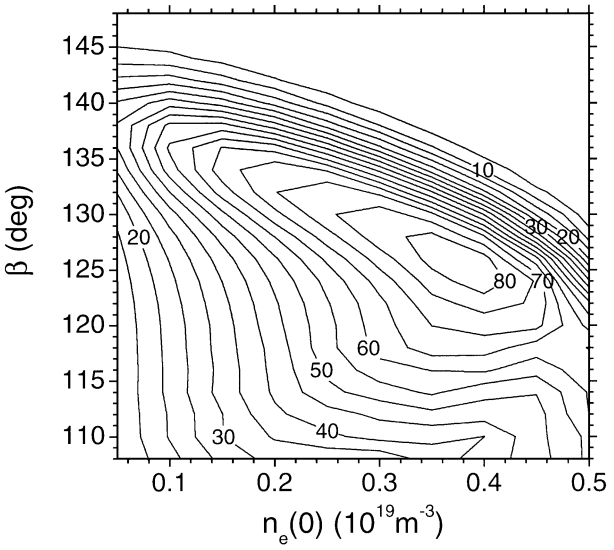

Fig. 4. Contour plot of the total absorption rate as a function of electron density and poloidal injection angle. The electron temperature and the magnetic field are assumed to be $T_e(0) = 500\,\mathrm{eV}$ and $B(0) = 0.5\,\mathrm{T}$.

as a function of the density and the poloidal launching angle. The poloidal angle, β, is defined as the angle between the wave beam and the major axis at the mirror position. The angle, $\beta = 132\,\mathrm{deg}$, corresponds to the beam crossing the magnetic axis in vacuum. The higher accessible density with maximum absorption rate is obtained by adjusting the poloidal angle where most of the refracted waves cross the resonance layer. The drawback is that the absorption profile becomes broad due the stronger refraction.

Accessible plasma parameters can be predicted by combining the absorption results with the ISS95 energy confinement scaling law.[4] In these estimates, the absorbed power and the plasma parameters are consistently determined. The energy confinement time in the steady state is given by $\tau_E = 3/2 \int n_e T_e \mathrm{d}V / P_{abs}$. The contribution of ion components to the total stored energy is neglected, since the ion temperature is expected to be lower than the electron temperature at low density due to the low collisionality. We note that this assumption causes the underestimation of energy confinement time. Estimated plasma parameter ranges are $n_e(0) < 0.4 \times 10^{19}\,\mathrm{m}^{-3}$, $T_e(0) < 800\,\mathrm{eV}$ and $\tau_E < 5\,\mathrm{msec}$ for $B = 0.5\,\mathrm{T}$, $P = 200\,\mathrm{kW}$, $a = 0.2\,\mathrm{m}$ and $R = 1.2\,\mathrm{m}$. This confinement time is shorter than the available ECRH pulse length, 40 msec, so that the quasi-stationary plasma can be obtained.

The fundamental ordinary (O_-) mode heating has also been modeled using the H-RAY code. Although the accessible density is doubled, the calculated total absorption rate at $B = 1.0\,\mathrm{T}$ is low, around 20% due to the low absorption coefficient. Some improvement schemes may be required for effective heating. Installation of a reflecting mirror, which would reflect the non-absorbed power back into the plasma, could improve the absorption. A mode conversion process into the electron Bernstein (B) waves (O-mode — slow X-mode — B-mode or slow X-

mode — B-mode) may also be an effective means of improvement. The converted B waves are fully absorbed at the Doppler shifted cyclotron resonance even at low electron temperature.

Summarizing, the power absorption during the electron cyclotron heating in the H-1 heliac has been calculated using a ray tracing numerical code. Two launching schemes have been considered, horizontal and bottom launching. Calculation results show that the 28 GHz ECH is promising for the plasma production and heating at 0.5 T using the X-mode second-harmonic resonance. The maximum power absorption of 82% is obtained at the second harmonic X-mode heating at low density. A higher accessible density can be reached if the launching angle is properly adjusted. The accessible electron density and temperature and the energy confinement time are estimated by combining the results with the ISS95 energy confinement scaling law.

The bottom launching is preferable for higher single pass absorption. One physical problem may be a thermal refraction effect on the wave propagation. It has been pointed out theoretically that the refraction effect gives rise to the wave reflection at the resonance, even below the cut-off density, when the angle between $\boldsymbol{k}$ and B contour is smaller than a critical value.[12] A trade-off between the highly optical path and the reduction of the thermal refraction effect may be required. This effect should be investigated experimentally in the future.

The authors would like to thank the H-1 staff for their continuous discussion. The encouragement of Professors J. H. Harris and T. Obiki is appreciated. One of the authors (K. N.) was supported by the Overseas Research Fellowship of the Japanese Ministry of Education, Sports and Culture during his stay at ANU.

1) K. Matsuda: IEEE Trans. Plasma Sci. **17** (1989) 6.
2) R. C. Goldfinger and D. B. Batchelor: Nucl. Fusion **27** (1987) 31.
3) V. Tribaldos, J. A. Jiménez, J. Guasp and B. Ph. van Milligen: Plasma Phys. Control. Fusion **40** (1998) 2113.
4) U. Stroth, M. Murakami, R. A. Dory, H. Yamada, S. Okamura, F. Sano and T. Obiki: Nucl. Fusion **36** (1996) 1063.
5) S. M. Hamberger, B. D. Blackwell, L. E. Sharp and D. B. Shenton: Fusion Technol. **17** (1990) 123.
6) M. G. Shats, D. L. Rudakov, B. D. Blackwell, L. E. Sharp, R. Tumlos, S. M. Hamberger and O. I. Fedyanin: Nucl. Fusion **34** (1994) 1653.
7) T. H. Stix: Waves in Plasmas (AIP, New York, 1992) Chap. 4.
8) M. Bornatici, R. Cano, O. De Barbieri and F. Engelmann: Nucl. Fusion **23** (1983) 1153.
9) S. Nowak, E. Lazzaro and G. Ramponi: Phys. Plasmas **3** (1996) 4140.
10) A. G. Peeters, Phys. Plasmas **3** (1996) 4386.
11) K. Nagasaki, T. Mizuuchi, S. Besshou, H. Funaba, K. Ida, K. Kondo, H. Morioka, T. Obiki, H. Okada, F. Sano and H. Zushi: J. Phys. Soc. Jpn. **67** (1998) 1625.
12) D. C. McDonald, R. A. Cairns, C. N. Lashmore-Davies and G. Le Clair: Phys. Plasmas **5** (1998) 883.